1

2

3

SARS-CoV-2-associated ssRNAs activate inflammation and

4

immunity via TLR7/8

5

6   **Valentina Salvi[1], Hoang Oanh Nguyen[1], Francesca Sozio[1,2], Tiziana Schioppa[1,2], Mattia Laffranchi[1],**

7   **Patrizia Scapini[3], Mauro Passari[1], Ilaria Barbazza[1], Laura Tiberio[1], Nicola Tamassia[3], Cecilia**

8   **Garlanda[2,4], Annalisa Del Prete[1,2], Marco A. Cassatella[3], Alberto Mantovani[2,4,5],*, Silvano Sozzani[6],***

9   **and Daniela Bosisio [1],***

10

11   [1] Department of Molecular and Translational Medicine, University of Brescia, Italy

12   [2] IRCCS Humanitas Research Hospital, Rozzano (MI), Italy.

13   [3] Department of Medicine, Section of General Pathology, University of Verona, Italy

14   [4] Department of Biomedical Sciences, Humanitas University, Pieve Emanuele (MI), Italy.

15   [5] The William Harvey Research Institute, Queen Mary University of London, London, UK.

16   [6] Laboratory Affiliated to Istituto Pasteur Italia-Fondazione Cenci Bolognetti, Department of

17   Molecular Medicine, Sapienza University of Rome, Rome, Italy

18   * Correspondence: daniela.bosisio@unibs.it; silvano.sozzani@uniroma1.it;

19   alberto.mantovani@humanitasresearch.it

20   **Running title:** SARS-CoV-2-specific PAMPs activate TLR7 and TLR8

21

22   **Abstract**

23   The inflammatory and IFN pathways of innate immunity play a key role in both resistance and

24   pathogenesis of Coronavirus Disease 2019 (COVID-19). Innate sensors and SARS-CoV-2-Associated

25   Molecular Patterns (SAMPs) remain to be completely defined. Here we identify single-stranded RNA

26   (ssRNA) fragments from SARS-CoV-2 genome as direct activators of endosomal TLR7/8 and MyD88

27   pathway. The same sequences induced human DC activation in terms of phenotype and functions,

28   such as IFN and cytokine production and Th1 polarization. A bioinformatic scan of the viral genome

29   identified several hundreds of fragments potentially activating TLR7/8, suggesting that products of

30   virus endosomal processing potently activate the IFN and inflammatory responses downstream these

31   receptors. In vivo, SAMPs induced MyD88-dependent lung inflammation characterized by

32   accumulation of proinflammatory and cytotoxic mediators and immune cell infiltration, as well as

33   splenic DC phenotypical maturation. These results identify TLR7/8 as crucial cellular sensors of

34   ssRNAs encoded by SARS-CoV-2 involved in host resistance and disease pathogenesis of COVID-19.

35

36

37   **Keywords:** Pattern Recognition Receptors, Pathogen Associated Molecular Patterns, cytokine

38   storm, Type I IFN, dendritic cells.

39

40

Introduction

41   SARS coronavirus 2 (SARS-CoV-2), is a positive-sense ssRNA virus belonging to the family of

43   Coronaviridae, also including the closely related Middle East respiratory syndrome coronavirus

44   (MERS-CoV) and SARS-CoV **(1)**. In a subgroup of patients, SARS-CoV-2 infection (Coronavirus

45   disease 2019, COVID-19) develops as acute respiratory distress syndrome featuring intense lung

46   injury, sepsis-like manifestations and multi-organ failure (2) associated with overt production of pro-

47   inflammatory cytokines that directly correlates with poor prognosis (3). This clinical condition

48   suggests that an overactive innate immune response may unleash virus-dependent immune

49   pathology (4). Innate immune activation is also responsible for inducing the protective antiviral state,

50   largely mediated by the release of type I IFNs. Indeed, inborn errors in type I IFN production and

51   amplification (5) or pre-existing blocking auto-antibodies against members of the IFN family of

52   cytokines (6) were found to correlate with unfavorable prognosis.

53   DCs act as crucial messengers linking innate and adaptative immunity against viral infections

54   (7, 8). Within DC heterogeneity, plasmacytoid DCs (pDCs) play an important role as the major source

55   of type I IFN in response to viral infection, while conventional DCs (cDCs) respond to a vast variety

56   of pathogens by producing pro-inflammatory cytokines and are the main responsible for T cell

57   activation (9–11). pDCs sense ssRNA viruses through TLR7 (12), an endosomal receptor activated by

58   genomic fragments rich in guanine (G) and uracil (U), derived by endosomal processing of the virus

59   independently of infection (13). By contrast, cDCs express the closely related TLR8 (14). Despite the

60   fact that TLR7 and TLR8 display high structural and functional homology, similar ligand specificity

61   (15) and recruit the same signaling intracellular adaptor molecule, MyD88 (16), the signaling

62   pathways of these two TLRs diverge in the functional significance, with TLR7 more involved in the

63   antiviral immune response and TLR8 mastering the production of pro-inflammatory cytokines. Both

64   cDCs and pDCs were shown to be reduced in the blood of severe acute COVID-19 patients (17, 18) as

65   a possible result of cell activation (19), but the mechanisms of SARS-CoV-2 recognition and activation

66   by innate immune cells still need to be identified. This study characterizes the first SARS-CoV-2-

67   associated molecular patterns (SAMPs) and identifies the TLR7/8/MyD88 axis as a crucial pathway

68   in the activation of human pDCs and cDCs.

69   Results

70   *Identification of potential ssRNA SAMPs*

71   Based on previous work identifying RNA40, a ssRNA rich in guanine and uracil (GU-rich) from

72   the U5 region of HIV-1, as the first natural agonist of TLR7 and TLR8 (20) and on known features of

73   TLR7/8 ligands (15, 21, 22), we searched for putative immunostimulatory sequences within the SARS-

74   CoV-2 ssRNA genome. Our bioinformatic scan revealed 491 GU-rich sequences, among which more

75   than 250 also bearing at least one "UGUGU" Interferon Induction Motif (IIM) (15, 20, 21) (Suppl. Table

76   1).

77   We hypothesized that these sequences may represent so far unidentified SAMPs responsible for

78   viral recognition and immune activation via endosomal TLR triggering. The elevated number of

79   sequences detected suggests that, upon endosomal engulfment, the fragmentation of the SARS-CoV-2

80   genome may generate many TLR7/8-triggering sequences, thus displaying high chances to contact and

81   activate the IFN and inflammatory responses downstream these receptors.

82   To validate the stimulatory potential on innate immune cells, two representative sequences, SCV2-

83   RNA1 and SCV2-RNA2, were chosen within the previous list, synthesized and tested in *in vitro* and *in*

84   *vivo* models of inflammation.

85

86   *ssRNA SAMPs activate human monocyte-derived DCs (moDCs)*

87   moDCs, a model of inflammatory cDCs expressing a wide variety of TLRs (7, 23–25), were treated

88   with increasing concentrations of SCV2-RNA1 and SCV2-RNA2 along with HIV-1-derived RNA40

89   (Heil 2004), used as a positive control. U/A alternated control sequences SCV2-RNA1A and SCV2-

90   RNA2A were used as negative controls (see materials and methods). Figure 1A shows that both

91   fragments efficiently activated cytokine secretion by moDCs. In particular, we observed potent

92   induction of pro-inflammatory cytokines (TNF-α, IL-6), of the Th1-polarizing cytokine IL-12 and

93   chemokines recruiting polymorphonuclear neutrophils (CXCL8), myelomonocytic cells (CCL3) and

94   Th1- and cytotoxic effectors cells (CXCL9). Especially at low concentrations, SCV2-RNA1 and SCV2-

95   RNA2 were more efficient than HIV-1-derived RNA40. In all experimental conditions, U/A alternated

96   SCV2-RNA1A and SCV2-RNA2A did not induce cytokine secretion. SCV2-RNA1 and SCV2-RNA2 also

97   induced moDC phenotypical maturation in terms of CD83, CD86 and CCR7 expression (Figure 1B).

98   Similarly to cytokine secretion, upregulation of maturation markers by RNA40 was less effective. These

99   results demonstrated that both SCV2-RNA1 and SCV2-RNA2 behave as SAMPs endowed with potent

100 DC stimulatory capacity. Because of their similar potency, further experiments were carried out using

101 a mixture of the two SAMPs (indicated as SCV2-RNA), a condition that may also better mimic a

102 physiological stimulation by multiple sequences derived from SARS-CoV-2 genome endosomal

103 fragmentation.

104

105 *ssRNA SAMPs activate T cell responses*

106   The impact of SAMPs on the ability of DCs to stimulate T cell functions was investigated in co-

107 culture experiments of SAMP-activated DCs with allogeneic naïve CD4$^+$ and CD8$^+$ T cells. Figure 2A

108 shows that SAMP-activated DCs induced proliferation of both naïve CD4$^+$ (left) and CD8$^+$ (right) T

109 cells. Activated CD4$^+$ T cells produced IFN-γ but no IL-4, a typical Th1-effector phenotype (Figure

110 2B). Functional activation of CD8$^+$ T cells was similarly demonstrated by the detection of secreted

111 IFN-γ (Figure 2C, left panel) and the intracellular accumulation of Granzyme B (GrB, right panel), a

112 marker of a cytotoxic phenotype. None of these effects were observed when DCs were activated with

113 U/A alternated SAMPs.

114   These experiments demonstrated that phenotypical DC maturation induced by SAMPs (Figure 1B)

115 is paralleled by the acquisition of T-cell activating capabilities. Thus, SAMPs have the ability to induce

116 a Th1-oriented immune response.

117

118 *ssRNA SAMPs activate human primary DCs*

119   The ability of SCV2-RNAs to activate DCs was further investigated using primary circulating cDCs

120   (comprising CD141+ cDC1 and CD1c+ cDC2) and BDCA2+ pDCs. SCV2-RNA efficiently induced the

121   secretion of TNF-α and IL-6 (Figure 3A) and the expression of maturation markers, such as CD86 and

122   CCR7 (Figure 3B) in cDCs. Similarly, SAMPs stimulated the release of IFN-α and TNF-α by pDCs

123   (Figure 3C), as well as their maturation in terms of CD86 upregulation and BDCA2 reduction (Figure

124   3D). Similarly to previous results, U/A alternated control sequences did not activate cytokine

125   production or maturation in either pDCs and cDCs (not shown).

126

127   *ssRNA SAMPs act as TLR7/8 ligands*

128   Despite the fact that SARS-CoV-2 has been shown to activate immune cells, the cellular sensors

129   responsible for viral detection are still ill defined. To formally demonstrate the ability of SAMPs to

130   functionally activate TLRs, experiments were performed in HEK-293 cells stably transfected with

131   human TLR7 and TLR8 together with a NF-κB reporter gene. Figure 4A depicts the activation of NF-

132   kB and luciferase production in both TLR7- and TLR8-expressing cells by SAMPs. Since both TLR7 and

133   TLR8 signal through the common adaptor MyD88, siRNA interference was performed in moDCs.

134   Figure 4B (left panel) shows that two different MyD88-specific siRNAs could decrease by about 50%

135   the levels of MyD88 mRNA, while the expression of the TLR3-related adaptor TRIF was not affected.

136   Consistent with this result, IL-6 production by SCV2-RNA was also decreased, whereas the stimulation

137   of moDCs by Poly I:C was not affected (Figure 4B right panel). Next, moDCs were stimulated in the

138   presence of CU-CPT9a, a specific TLR8 inhibitor (26). CU-CPT9a inhibited in a potent and dose-

139   dependent manner the release of IL-6 when cells were stimulated with SCV2-RNA or R848 (TLR7/8

140   ligand). On the other hand, the TLR8 inhibitor did not affect the stimulation by LPS, a TLR4 ligand

141   (Figure 4C). The complete inhibition observed upon TLR8 blocking is not surprising given the low

142   expression of TLR7 in moDCs (23). TLR7 and TLR8 display a mutual exclusive expression in primary

143   DCs. Indeed, cDCs express TLR8 as their unique endosomal ssRNA receptor, while pDCs express TLR7

144   (14). Consistent with this, CU-CPT9a blocked the production of pro-inflammatory cytokines in cDCs

145   (Figure 5A). Our effort to block TLR7 signaling using commercially available receptor antagonists was

146   unsuccessful since none of these inhibitors blocked TLR7 activation in pDCs stimulated with R848 or

147   Imiquimod (data not shown). As an alternative strategy to demonstrate the involvement of TLR7 in

148   SCV2-RNA sensing we performed TLR desensitization (21). pDCs were stimulated with SCV2-RNA or

149   R848 or left untreated, washed, and then re-stimulated with R848. Figure 5B shows that, upon re-

150   stimulation, only untreated cells could respond to R848 in terms of IFN-α and TNF-α production as a

151   result of TLR7 desensitization by its ligand R848 as well as by SCV2-RNA. The limited yield following

152   blood DC purification hampered the use of MyD88 siRNA. However, the involvement of endosomal

153   TLRs as SCV2-RNA receptors was further supported by the blocking of cytokine release in both cDCs

154   (Figure 5C) and pDCs (Figure 5D) by chloroquine (CQ), a drug known to block endosomal TLR

155   triggering by interfering with endosomal acidification (27).

156

157   *ssRNA SAMPs induce DC activation and lung inflammation in vivo*

158   To address the capacity of SAMPs to induce inflammation and immune activation *in vivo*, we

159   first investigated if SAMPs can also trigger murine TLRs. TLR expression was analyzed in RAW264.7,

160   a murine cell line, showing the expression of the ssRNA receptor TLR7 among other TLRs (Figure

161   6A). These TLR7-bearing cells responded to SAMP stimulation by producing TNF-α and this effect

162   was blocked by CQ (Figure 6B) confirming that SCV2-RNA activate murine cells, presumably via

163   TLR7. In addition, splenocytes from MyD88^{-/-} mice did not produce pro-inflammatory cytokines

164   when stimulated with SCV2-RNA despite expressing similar levels of TLRs (Figure 6C and D). Based

165   on these results, C57Bl6/J WT and MyD88$^{-/-}$ mice were injected i.v. with SAMPs or vehicle and

166   sacrificed 6 hours later. A significant increase of type I IFN was detected in the sera of WT SAMP-

167   treated mice indicating systemic immune activation (Figure 6E). Consistent with this, SAMPs

168   induced the upregulation of CD40 and CD86 on splenic pDCs (CD11c^{int}MHC-II$^+$B220$^+$SiglecH$^+$)

169   (Figure 6F). Activation of splenic cDC1s (CD11c$^+$MHC-II$^+$CD8α^+CD11b$^-$) and cDC2s (CD11c$^+$MHC-II$^+$

170   CD8α^-CD11b$^+$) was also detected (Figure 6G and H). Figure 7A shows that SAMP treatment induced

171   the expression of pro-inflammatory cytokines TNF-α, IL-1β and IL-6 and of IFN-α and IFN-γ in the

172   lung. In addition, a marked increase in the expression of chemokines active on myeloid and Th1

173   effector cells (i.e. CCL3, CCL4 and CXCL10) was also detected. Conversely, CCL20 and CCL22, two

174   chemokines active in Th17 and Th2 T cell recruitment, were not increased (Figure 7B). We could also

175   detect the accumulation of molecules involved in cytotoxic tissue damage such as GrB and TRAIL

176   (Figure 7C) that, given the short kinetics of stimulation, may reflect the recruitment of NK cells to the

177   lungs. The increase of CD45 and MHC-II mRNA levels (data not shown) further suggested immune

178   cell infiltration, which was confirmed by histological analysis. Lung histology revealed a marked

179   infiltration of inflammatory cells into peri-bronchial and peri-vascular connective tissue and alveolar

180   septal thickening in SAMP-treated mice (Figure 7D). On the contrary, SAMP administration to

181   MyD88$^{-/-}$ mice did not induce any inflammatory response, including the increase of circulating levels

182   of type I IFN, DC maturation and the generation of a lung infiltrate (Fig. 6 D-H and Figure 7). These

183   data extend to the *in vivo* condition the observation that SAMPs use a TLR/MyD88-dependent

184   pathway to trigger a type I IFN/pro-inflammatory activation program and highlight lung as a

185   primary target organ.

186

SARS-CoV-2-specific PAMPs activate TLR7 and TLR8   Salvi et al., page 10 of 26

Discussion

187

188   Here, we report that two short sequences within the ssRNA genome of SARS-CoV-2 activate the

189   production of type I IFNs and the T cell-activating ability of human DCs by triggering endosomal

190   TLR7 and TLR8. Of note, these sequences represent prototypical examples of the several hundreds of

191   potential TLR ligands identified by SARS-CoV-2 genome scan. This finding is in line with previous

192   work demonstrating a twenty-fold higher density of GU-rich fragments in the closely related SARS-

193   CoV as compared to HIV-1 (28) and with a recent bioinformatic study showing that SARS-CoV-2

194   encodes a number of such fragments even larger than SARS-CoV (29). Thus, endosomal processing

195   of SARS-CoV-2 nucleic acids may give rise to multiple fragments endowed with the property to

196   trigger innate immune activation.

197   DCs play a crucial role as activators of both inflammation and adaptive immune responses (7,

198   8) and pDCs are the major producers of type I IFNs in response to viral infections (10–12). The

199   protective role of type I IFN in life-threatening COVID-19 has been documented based on the clinical

200   outcome of patients with inborn errors in type I IFN immunity or producing blocking auto-Abs against

201   different types of type I IFNs (5, 6). Therefore, SAMPs may represent one of the essential signals in

202   the activation of an IFN response and Th1-oriented adaptive immunity (30, 31). In this regards it is

203   of note that SARS-CoV-2 infection affected the number of pDCs in vivo (17, 18) and primary virus

204   isolates induced the activation of pDCs, *in vitro* (32). Here we extend this knowledge through the

205   identification of viral sequences active on pDCs as well as cDCs and moDCs and show that the

206   activation program induced by SAMPs is not restricted to type I IFNs, but encompassed the

207   production of pro-inflammatory cytokines and the generation of Th1-oriented responses, supporting

208   a possible role for these cells in the generation of the exuberant pro-inflammatory response observed

209   in life-threatening COVID-19(33).

210   Very rare loss-of-function variants of TLR7 in two independent families was associated with severe

211   COVID-19 in males (34). Thus, our report on the ability of SAMPs to activate the TLR7/8 and MyD88

212   pathways provides the missing link between this clinical evidence and our molecular knowledge on

213   the cellular sensors for SARS-CoV-2 detection. Viral recognition by endosomal TLRs takes place before

214   and independently of infection, as a consequence of pathogen endocytosis (13). Indeed, pDCs were

215   reported to be resistant to infection, although they were activated by SARS-CoV-2 (32). This is an

216   important process that gives innate immune cells the opportunity to activate early antiviral response.

217   It remains to be elucidated if SARS-CoV-2 uptake for endosomal processing is a direct process or

218   mediated by receptors, such as ACE2 or CD147 (35). ssRNA-sensing TLRs are expressed also by other

219   innate immune cells, such as macrophages, as well as by peripheral tissues such as lung, bronchus,

220   rectum, and cerebral cortex (36). Thus, other cells may support as well both protective and excessive

221   antiviral responses (4). Since the magnitude of TLR activation differs in individuals, such as elderly

222   people, differences in TLR activation may help explain differences in the quality of the antiviral

223   immune response independently of SAMP potency (37).

224   By all means, other SAMPs and DAMPs as well as the simultaneous engagement of different

225   PRRs are likely to contribute to COVID-19-associated protective response and cytokine storm,

226   including cytosolic sensors, such as retinoid-inducible gene-1 (RIG1)-like receptors **(38)**, Interferon

227   Induced proteins with tetratricopeptide repeats, or members of a large group of RNA-binding

228   molecules with poorly defined ligand specificity **(38)**. A search for specific candidate ligands of cytosolic

229   RNA-sensors was hampered because the scarce definition of their ligand consensus sequences.

230   However, the finding that SARS-CoV-2 can evade innate immune restriction provided by intracellular

231   RNA-sensors via methylation the 5'-end of its cellular mRNAs **(39)** further reinforces the role for TLRs

232   as crucial sentinels and regulators of immune response to SARS-CoV-2 infection. SARS-CoV-2 is known

233   to induce inflammasome assembly despite the exact mechanism still need to be characterized (40, 41).

234   Since intracellular nucleic acid sensors are known to activate inflammasomes (42), and TLR activation

235 is intimately connected with inflammasome functions (43), it is possible that SCV2-RNAs used in this

236 study may also contribute to activate this pathway.

237   In conclusion, this work describes that SARS-CoV-2 is as a potential powerful source of

238 immunostimulatory nucleic acid fragments and identifies the first SARS-CoV-2-specific PAMPs

239 endowed with the ability to promote inflammation and immunity triggering TLR7 and TLR8. Based

240 on previous works demonstrating a) the crucial protective role of type I IFNs against COVID-19 (5,

241 6); b) the crucial protective role of TLR7 against life-threatening SARS-CoV-2 infection (34) and c)

242 pDC activation *in vitro* by SARS-CoV-2 (32), we believe that our findings fill a gap in the

243 understanding of SARS-CoV-2 host-pathogen interaction.

244

245   **Methods**

246   *Identification of potential TLR7/8-triggering ssRNA PAMPs*

247   The reference SARS-CoV-2 genome (NC_045512, positive strand) was scanned for GU-rich ssRNA

248   fragments with the SequenceSearcher tool in the Fuzzy mode (44). We defined "GU-enriched

249   sequences" short strings with a maximal length of 20 bp, that were composed for more than 40% of the

250   length by "GU" and/or "UG" pairs. The identified 491 GU-rich sequences were further selected based

251   on the content of at least one "UGUGU" Interferon Induction Motif (IIM)(21) (see Suppl. Table 1).

252   Within this list, the following were selected and synthesized by Integrated DNA Technologies (IDT)

253   for subsequent studies: SCV2-RNA1 5'-UGCUGUUGUGUGUU*U-3' (genome position: 15692-15706);

254   SCV2-RNA2 5'-GUGUGUGUGUUCUGUUAUU*G-3' (genome position: 20456-20475). These

255   sequences were checked for uniqueness with BLAST in the database RefSeq Genome Database

256   (refseq_genomes) within the RNA viruses (taxid: 2559587). Two additional sequences were

257   synthesized, in which "U" was substituted with "A", in order to impair TRL7/8 stimulation (SCV2-

258   RNA1A and SCV2-RNA2A) (15, 20). * indicates a phosphorothioate linkage.

259

260   *Cell preparation and culture*

261   Buffy coats from blood donations of anonymous healthy donors were obtained and preserved by the

262   Centro Trasfusionale, Spedali Civili of Brescia according to the italian law concerning blood

263   component preparation and analysis. Peripheral blood mononuclear cells (PBMC) were obtained by

264   density gradient centrifugation and monocytes were subsequently purified by immunomagnetic

265   separation using anti CD14-conjugated magnetic microbeads (Miltenyi Biotec) according to the

266   manufacture's protocol and as previously published (23). Briefly, monocytes were cultured for 6 days

267   in tissue culture plates in complete medium (RPMI 1640 supplemented with 10% heat-inactivated,

268   endotoxin free FBS, 2 mM L-Glutamine, penicillin and streptomycin (all from Gibco, Thermo Fisher

269　Scientific) in the presence of 50 ng/ml GM-CSF and 20 ng/ml IL-4 (Miltenyi Biotec). Untouched

270　peripheral blood cDC1 and cDC2 (cDCs) and pDCs were obtained from PBMC after negative

271　immunomagnetic separation with the Myeloid Dendritic Cell Isolation kit (Miltenyi Biotec) and the

272　Plasmacytoid Dendritic Cell Isolation kit II (Miltenyi Biotec), respectively. pDCs were cultured in

273　completed RPMI medium with 20 ng/ml IL-3 (Miltenyi Biotec). RAW264.7 cells were purchased from

274　American Type Culture Collection and cultured in DMEM complemented with 10% FBS.

275

276　**Cell stimulation with viral RNAs**

277　Complexation of RNA with DOTAP Liposomal Transfection Reagent (Roche) was performed as

278　previously described (21). Briefly, 5 μg RNA in 50 μl HBS buffer (20 mM HEPES, 150 mM NaCl, pH

279　7.4) was combined with 100 μl DOTAP solution (30 μl DOTAP plus 70 μl HBS buffer) and incubated

280　for 15 minutes at RT. Where indicated, cells were pretreated for 1 hour with Chloroquine or CU-

281　CPT9a or stimulated with TLR agonists (all from Invivogen).

282

283　**MyD88 silencing in moDCs**

284　Differentiating monocytes at day 2 of culture were transfected with two different MyD88 Silencer

285　Select Validated siRNA or with a control siRNA (all at 50 nM final concentration; Ambion, Thermo

286　Fisher Scientific) using Opti-MEM I reduced serum medium and Lipofectamine RNAiMAX

287　transfection reagent (Thermo Fisher Scientific) as previously described (45). Transfected cells were

288　incubated for 72 hours and then stimulated for 24 hours with TLR agonists as indicated. The effects

289　of mRNA silencing by siRNA was investigated by real-time PCR using specific QuantiTect primer

290　Assay (Qiagen).

291

Cytokine detection

293 TNF-α, IL-6, IL-12p70, CXCL8, CXCL9, CCL3 and mouse TNF-α were measured by ELISA assay

294 (R&D Systems). Human IFN-α was detected using specific Module Set ELISA kit (eBioscience).

295 Mouse IFN-α was measured by a bioluminescence kit (InvivoGen). All assays were performed on cell

296 free supernatants according to the manufacturer's protocol.

297

Flow cytometry

299 Human and mouse DCs were stained with the following antibodies from Miltenyi Biotec or as

300 specified: Vioblue-conjugated anti-human CD86 (clone FM95, Miltenyi Biotec), PE-conjugated anti-

301 human CD83 (clone REA714), FITC-conjugated anti-human BDCA2 (clone AC144), APC-conjugated

302 anti-human CCR7 (clone REA546), VioGreen-conjugated anti-mouse CD45 (clone REA737), VioBlue

303 or FITC-conjugated anti-mouse MHCII (clone REA564), PerCP-Vio 700-conjugated anti-mouse

304 CD11c (clone REA754), PE-conjugated anti-mouse SiglecH (clone 551.3D3), PE-Vio 615-conjugated

305 anti-mouse CD11b (clone REA592), VioBlue-conjugated anti-mouse CD8a (cloneREA601), PE-Vio

306 770-conjugated anti-mouse B220 (clone RA3-6B2), PE-conjugated anti-mouse CD40 (clone REA965),

307 FITC-conjugated anti-mouse CD40 (clone HM40-3, Biolegend) and APC-CY7-conjugated anti-mouse

308 CD86 (clone GL-1, Biolegend). Samples were read on a MACSQuant Analyzer (Miltenyi Biotec) and

309 analysed with FlowJo (Tree Star Inc.). For intracellular detection of Granzyme B, cells were fixed and

310 permeabilized using the Inside Stain kit (Miltenyi Biotec) and stained with APC-conjugated anti-

311 Granzyme B (clone REA226, Miltenyi Biotec). Cell viability was assessed by LIVE/DEAD staining

312 according to the manufacturer's instruction (Molecular Probes, Thermo Fisher Scientific).

313

NF-κB luciferase reporter assay

TLR-specific activation assays were performed using human HEK293 cells expressing luciferase

under control of the NF-κB promoter and stably transfected with human TLR7 and TLR8 as

previously described (21). Briefly, 25000 cells were seeded in complete DMEM without antibiotics in

96-well plates for 24 hours and then stimulated with 10 μg/ml SCV2-RNA for additional 24 hours.

After stimulation, cells were lysed using ONE-Glo EX Luciferase Assay System (Promega) according

to the manufacturer's recommendations and assayed for luciferase activity using the

EnSightMultimode Plate Reader (PerkinElmer). HEK293-transfected cells were maintained in DMEM

supplemented with 10% FBS and specific antibiotics were added.

323

T cell proliferation assay

Experiments using T cells were conducted according to the "Minimal Information about T Cell

Assays" (MIATA) guidelines. Allogenic naïve CD4+ T cells and CD8+ T cells were isolated from

buffycoats using the naïve CD4+ T cell Isolation kit II (Miltenyi Biotec) and CD8+ T cell Isolation kit

(Miltenyi Biotec), respectively. Purified T cells were counted by flow cytometry and labeled with

CellTrace-CFSE (Molecular Probes, Thermo Fisher Scientific) at a final concentration of 5 μM.

Subsequently, T cells (1x105 cells/well) were cocultured with graded numbers of allogeneic moDCs

in 96-well round-bottom culture plates in complete RPMI medium. After 6 days, alloreactive T cell

proliferation was assessed by measuring the loss of the dye CellTrace-CFSE upon cell division using

flow cytometry. Positive controls of T cell proliferations were routinely performed using IL-2 plus

PHA. Response definition criteria were defined post-hoc. Dead cells were excluded by LIVE/DEAD

335   staining according to the manufacturer's instruction. These experiments were performed using

336   general research investigative assays. Raw data can be provided per request.

337

338   **Analysis of T cell cytokine production**

339   After 6 days of coculture, helper T cells were restimulated with 200 nM PMA (Sigma-Aldrich) plus 1

340   µg/ml of ionomycin (Sigma) for 5 hours. Brefeldin A (5 µg/ml, Sigma) was added during the last 2

341   hours. For intracellular cytokine production, cells were fixed and permeabilized with Inside Stain kit

342   (Miltenyi Biotec) and stained with FITC-conjugated anti-IFN-γ (clone 45-15, Miltenyi Biotec) and PE-

343   conjugated anti-IL-4 (clone 7A3-3, Miltenyi Biotec) following the manufacturer's recommendations.

344   For $CD8^+$ T cells, after 6 days of coculture, IFN-γ production was assessed in the culture supernatants

345   by ELISA (R&D system). Response definition criteria were defined post-hoc. These experiments were

346   performed using general research investigative assays. Raw data can be provided per request.

347

348   *In vivo* **experiments**

349   Procedures involving animal handling and care conformed to protocols approved by the University of

350   Verona in compliance with national (D.L. N.116, G.U., suppl. 40, 18-2-1992 and N. 26, G.U. March 4,

351   2014) and international law and policies (EEC Council Directive 2010/63/EU, OJ L 276/33, 22-09-2010;

352   National Institutes of Health Guide for the Care and Use of Laboratory Animals, U.S. National Research

353   Council, 2011). The study was approved by the Italian Ministry of Health (approval number 339/2015-

354   PR). Sex and age matched C57Bl6/J mice were obtained by Charles River Laboratories and housed in

355   the specific pathogen-free animal facility of the Department of Medicine, University of Verona. MyD88-

356   /- mice were kindly provided by S. Akira (Osaka University, Osaka, Japan). Mice were anesthetized with

357　isoflurane and injected i.v. in the retro-orbital vein with 300 μl DOTAP/SCV2-RNA mixture (20

358　μg/mouse) or with DOTAP alone. After 6 hours, mice were sacrificed and lungs, spleen and blood were

359　harvested. Briefly, lungs were collected upon intracardiac perfusion with cold PBS. Left lung lobes were

360　formalin fixed for 24 hours, dehydrated, and paraffin embedded for histological analysis. Right lungs

361　were immediately frozen at -80°C and used for real-time PCR. Spleens were mechanically and

362　enzymatically treated to obtain a single-cell suspension for cytofluorimetric and real-time PCR analysis.

363　All mouse experiments were carried out in accordance with guidelines prescribed by the Ethics

364　Committee for the use of laboratory animals for research purposes at the University of Verona and by

365　the Italian Ministry of Health. All efforts were made to minimize the number of animals used and their

366　suffering.

367

368　**Lung histological analysis**

369　Histology was performed on three longitudinal serial sections (150 μm apart, 4 μm in thickness) from

370　each left lung, stained with hematoxylin and eosin (H&E), and scanned by VS120 Dot- Slide BX61

371　virtual slide microscope (Olympus Optical) as previously described (46).

372

373　**Real-time PCR**

374　RNA was extracted using TRIzol reagent, treated with DNAse according to the manufacturer's

375　instructions and reverse transcription performed using random hexamers and MMLV RT (all from

376　Thermo Fisher Scientific). The SsoAdvanced Universal SYBR Green Supermix (Bio-Rad Laboratories)

377　was used according to the manufacturer's instructions. Reactions were run in triplicate on a StepOne

378　Plus Real-Time PCR System (Applied Biosystems) and analyzed by the StepOne Plus Software

379   (Version 2.3, Applied Biosystems). Sequences of gene-specific primers are available upon request.

380   Gene expression was normalized based on RPL32 mRNA content.

381

382   **Statistical analysis**

383   Statistical significance among the experimental groups was determined using paired or unpaired

384   Student's *t* test or one-way ANOVA with Dunnet's post-hoc test (GraphPad Prism 7, GraphPad

385   Software) as indicated in each figure legend. $P < 0.05$ was considered significant.

386

387

388

389

390

391

392

393

394

395

396

397

398

399

417

418

419   **References**

420   1. Zhu N et al. A Novel Coronavirus from Patients with Pneumonia in China, 2019. *N. Engl. J. Med.*

421   2020;382(8):727–733.

422   2. Guan W et al. Clinical Characteristics of Coronavirus Disease 2019 in China. *N. Engl. J. Med.*

423   2020;382(18):1708–1720.

424   3. Liu F et al. Prognostic value of interleukin-6, C-reactive protein, and procalcitonin in patients with COVID-

425   19. *J. Clin. Virol. Off. Publ. Pan Am. Soc. Clin. Virol.* 2020;127:104370.

426   4. Merad M, Martin JC. Pathological inflammation in patients with COVID-19: a key role for monocytes and

427   macrophages. *Nat. Rev. Immunol.* 2020;20(6):355–362.

428   5. Zhang Q et al. Inborn errors of type I IFN immunity in patients with life-threatening COVID-19. *Science*

429   2020;370(6515):eabd4570.

430   6. Bastard P et al. Autoantibodies against type I IFNs in patients with life-threatening COVID-19. *Science*

431   2020;370(6515):eabd4585.

432   7. Cabeza-Cabrerizo M, Cardoso A, Minutti CM, Pereira da Costa M, Reis E Sousa C. Dendritic Cells Revisited.

433   *Annu. Rev. Immunol.* [published online ahead of print: January 22, 2021]; doi:10.1146/annurev-immunol-061020-

434   053707

435   8. Sozzani S. Dendritic cell trafficking: More than just chemokines. *Cytokine Growth Factor Rev.* 2005;16(6):581–

436   592.

437   9. Villadangos JA, Schnorrer P. Intrinsic and cooperative antigen-presenting functions of dendritic-cell subsets

438   in vivo. *Nat. Rev. Immunol.* 2007;7(7):543–555.

439   10. Asselin-Paturel C et al. Type I interferon dependence of plasmacytoid dendritic cell activation and

440   migration. *J. Exp. Med.* 2005;201(7):1157–1167.

441   11. Blanco P, Palucka AK, Pascual V, Banchereau J. Dendritic cells and cytokines in human inflammatory and

442   autoimmune diseases. *Cytokine Growth Factor Rev.* 2008;19(1):41–52.

443   12. Swiecki M, Colonna M. The multifaceted biology of plasmacytoid dendritic cells. *Nat. Rev. Immunol.*

444   2015;15(8):471–485.

445   13. Uematsu S, Akira S. Toll-like Receptors and Type I Interferons. *J. Biol. Chem.* 2007;282(21):15319–15323.

446   14. Jarrossay D, Napolitani G, Colonna M, Sallusto F, Lanzavecchia A. Specialization and complementarity in

447   microbial molecule recognition by human myeloid and plasmacytoid dendritic cells. *Eur. J. Immunol.*

448   2001;31(11):3388–3393.

449   15. Shimizu T. Structural insights into ligand recognition and regulation of nucleic acid-sensing Toll-like

450   receptors. *Curr. Opin. Struct. Biol.* 2017;47:52–59.

451   16. Cervantes JL, Weinerman B, Basole C, Salazar JC. TLR8: the forgotten relative revindicated. *Cell. Mol.*

452   *Immunol.* 2012;9(6):434–438.

453   17. Zhou R et al. Acute SARS-CoV-2 Infection Impairs Dendritic Cell and T Cell Responses. *Immunity*

454   2020;53(4):864-877.e5.

455   18. Peruzzi B et al. Quantitative and qualitative alterations of circulating myeloid cells and plasmacytoid DC in

456   SARS-CoV-2 infection. *Immunology* 2020;161(4):345–353.

457   19. Sozzani S, Vermi W, Del Prete A, Facchetti F. Trafficking properties of plasmacytoid dendritic cells in

458   health and disease. *Trends Immunol.* 2010;31(7):270–277.

459   20. Heil F. Species-Specific Recognition of Single-Stranded RNA via Toll-like Receptor 7 and 8. *Science*

460   2004;303(5663):1526–1529.

461   21. Salvi V et al. Exosome-delivered microRNAs promote IFN-α secretion by human plasmacytoid DCs via

462   TLR7 [Internet]. *JCI Insight* 2018;3(10). doi:10.1172/jci.insight.98204

463   22. Diebold SS et al. Nucleic acid agonists for Toll-like receptor 7 are defined by the presence of uridine

464   ribonucleotides. *Eur. J. Immunol.* 2006;36(12):3256–3267.

465   23. Salvi V et al. TLR Signalling Pathways Diverge in Their Ability to Induce PGE2. *Mediators Inflamm.*

466   2016;2016:5678046.

467   24. Hornung V et al. Quantitative Expression of Toll-Like Receptor 1–10 mRNA in Cellular Subsets of Human

468   Peripheral Blood Mononuclear Cells and Sensitivity to CpG Oligodeoxynucleotides. *J. Immunol.*

469   2002;168(9):4531–4537.

470   25. Muzio M et al. Differential expression and regulation of toll-like receptors (TLR) in human leukocytes:

471   selective expression of TLR3 in dendritic cells. *J. Immunol. Baltim. Md 1950* 2000;164(11):5998–6004.

472   26. Zhang S et al. Small-molecule inhibition of TLR8 through stabilization of its resting state. *Nat. Chem. Biol.*

473   2018;14(1):58–64.

474   27. Kužnik A et al. Mechanism of Endosomal TLR Inhibition by Antimalarial Drugs and Imidazoquinolines. *J.*

475   *Immunol.* 2011;186(8):4794–4804.

476   28. Li Y et al. Extraordinary GU-rich single-strand RNA identified from SARS coronavirus contributes an

477   excessive innate immune response. *Microbes Infect.* 2013;15(2):88–95.

478   29. Moreno-Eutimio MA, López-Macías C, Pastelin-Palacios R. Bioinformatic analysis and identification of

479   single-stranded RNA sequences recognized by TLR7/8 in the SARS-CoV-2, SARS-CoV, and MERS-CoV

480   genomes. *Microbes Infect.* 2020;22(4–5):226–229.

481   30. Sharma NK, Sarode SC, Sarode G, Patil S. Is a COVID-19 vaccine developed by nature already at work?.

482   *Med. Hypotheses* 2020;145:110335.

483   31. Borges RC, Hohmann MS, Borghi SM. Dendritic cells in COVID-19 immunopathogenesis: insights for a

484   possible role in determining disease outcome. *Int. Rev. Immunol.* 2020;1–18.

485   32. Onodi F et al. SARS-CoV-2 induces human plasmacytoid pre-dendritic cell diversification via UNC93B and

486   IRAK4. *BioRxiv Prepr. Serv. Biol.* [published online ahead of print: January 8, 2021];

487   doi:10.1101/2020.07.10.197343

488   33. Zhang Q et al. Life-Threatening COVID-19: Defective Interferons Unleash Excessive Inflammation. *Med N.*

489   *Y. N* 2020;1(1):14–20.

490   34. van der Made CI et al. Presence of Genetic Variants Among Young Men With Severe COVID-19. *JAMA*

491   [published online ahead of print: July 24, 2020]; doi:10.1001/jama.2020.13719

492   35. Wang K et al. CD147-spike protein is a novel route for SARS-CoV-2 infection to host cells. *Signal Transduct.*

493   *Target. Ther.* 2020;5(1):283.

494   36. Papatheodorou I et al. Expression Atlas: gene and protein expression across multiple studies and

495   organisms. *Nucleic Acids Res.* 2018;46(D1):D246–D251.

496   37. Panda A et al. Age-associated decrease in TLR function in primary human dendritic cells predicts influenza

497   vaccine response. *J. Immunol. Baltim. Md 1950* 2010;184(5):2518–2527.

498   38. Chow KT, Gale M, Loo Y-M. RIG-I and Other RNA Sensors in Antiviral Immunity. *Annu. Rev. Immunol.*

499   2018;36(1):667–694.

500   39. Viswanathan T et al. Structural basis of RNA cap modification by SARS-CoV-2. *Nat. Commun.*

501   2020;11(1):3718.

502   40. Toldo S et al. Inflammasome formation in the lungs of patients with fatal COVID-19 [Internet]. *Inflamm. Res.*

503   [published online ahead of print: October 20, 2020]; doi:10.1007/s00011-020-01413-2

504   41. Rodrigues TS et al. Inflammasomes are activated in response to SARS-CoV-2 infection and are associated

505   with COVID-19 severity in patients. *J. Exp. Med.* 2021;218(3). doi:10.1084/jem.20201707

506   42. Xiao TS. The nucleic acid-sensing inflammasomes. *Immunol. Rev.* 2015;265(1):103–111.

507   43. Becker CE, O'Neill LAJ. Inflammasomes in inflammatory disorders: the role of TLRs and their interactions

508   with NLRs. *Semin. Immunopathol.* 2007;29(3):239–248.

509   44. Marass F, Upton C. Sequence Searcher: A Java tool to perform regular expression and fuzzy searches of

510   multiple DNA and protein sequences. *BMC Res. Notes* 2009;2:14.

511   45. Salvi V et al. Dual regulation of osteopontin production by TLR stimulation in dendritic cells. *J. Leukoc. Biol.*

512   2013;94(1):147–158.

513   46. Del Prete A et al. The Atypical Receptor CCRL2 Is Essential for Lung Cancer Immune Surveillance. *Cancer*
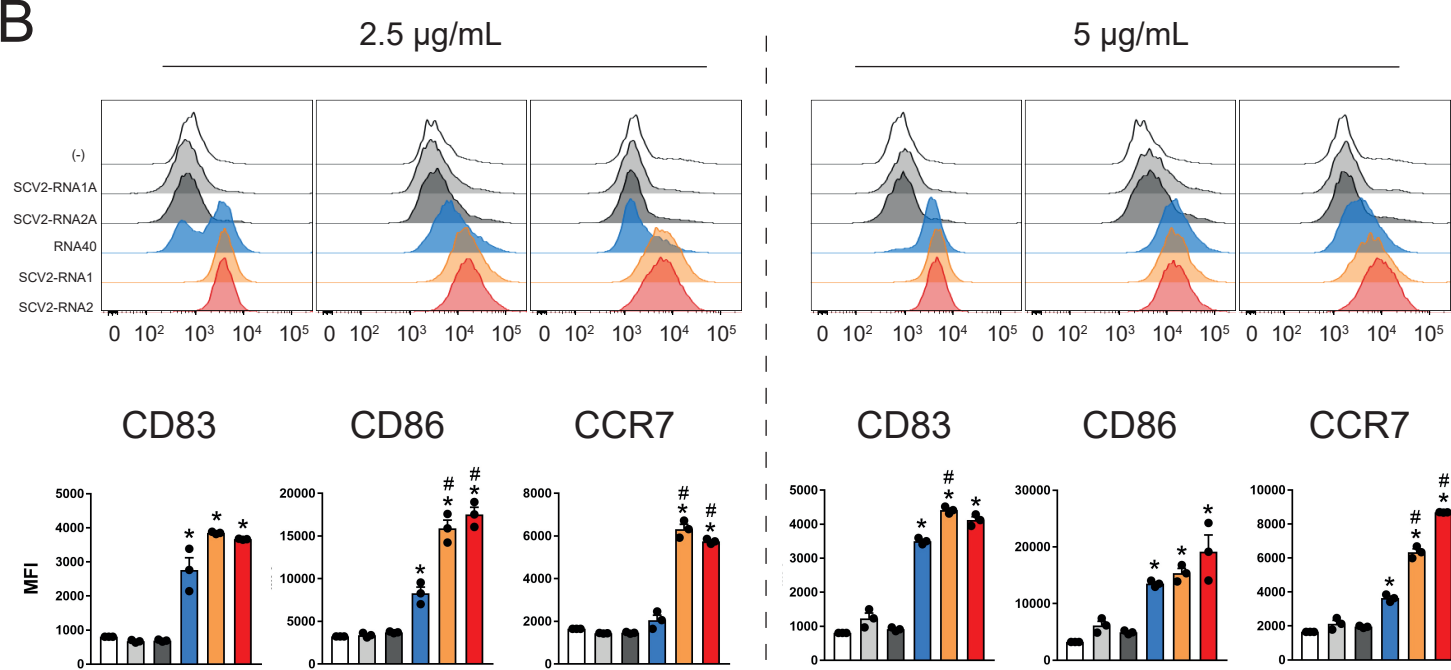
514   *Immunol. Res.* 2019;7(11):1775–1788.

515
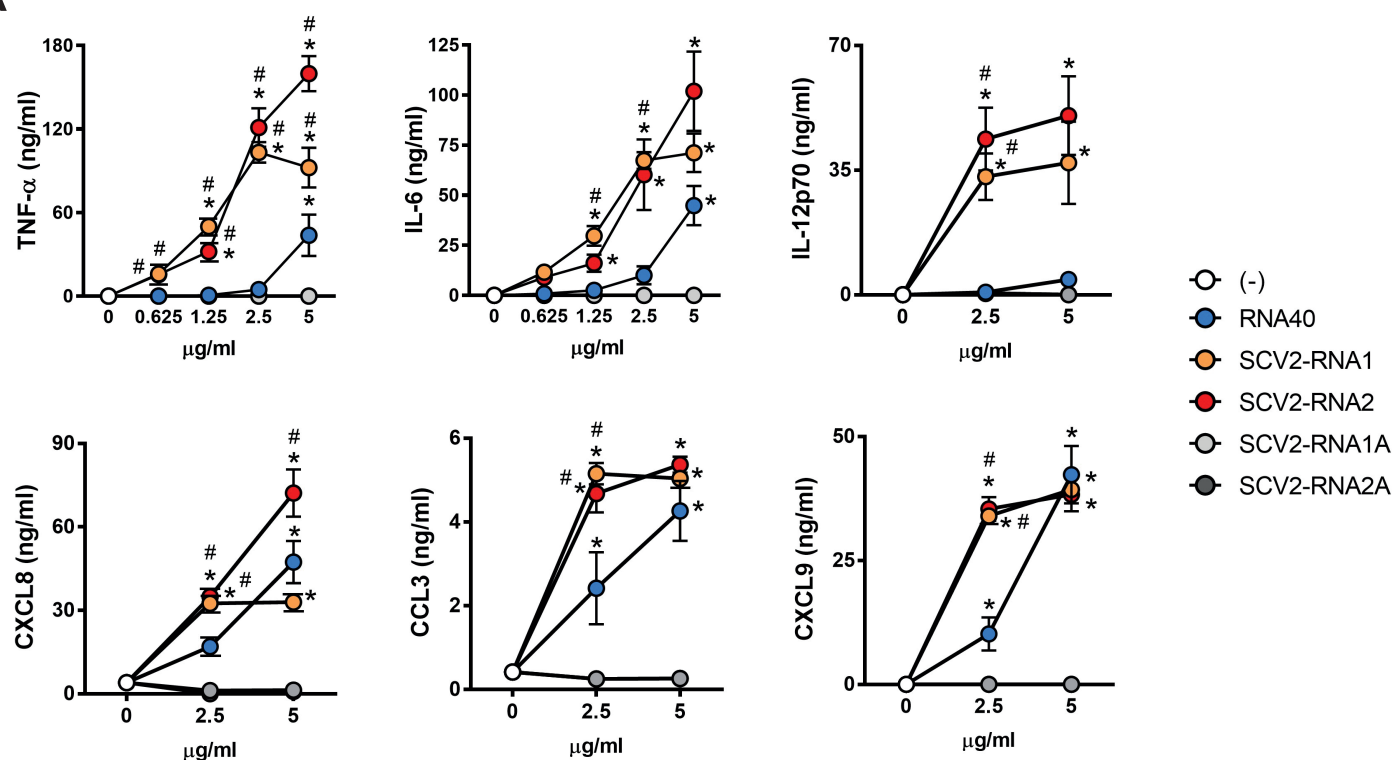
Figure 1. SAMPs activate cytokine secretion and phenotypical maturation of moDCs.
(A) moDCs (2x10⁶/ml) were stimulated with increasing concentrations of the indicated viral RNAs or with vehicle alone (-) for 24 hours. The production of TNF-α, IL-6, IL-12p70, CXCL8, CCL3 and CXCL9 was evaluated by ELISA in cell-free supernatants. Data are expressed as mean ± SEM (n=3). Results of SCV2-RNA1A and SCV2-RNA2A are superimposed in all graphs. (B) moDCs were stimulated as described in (A) and the surface expression of CD83, CD86 and CCR7 evaluated by FACS analysis. Data are expressed as representative cytofluorimetric profiles (upper panels) or as the mean ± SEM (n=3) of the Median of Fluorescence Intensity (MFI) (lower panels). (A-B) *P< 0.05 versus (-) by one-way ANOVA with Dunnett's post-hoc test; #P< 0.05 versus RNA40 by paired Student's *t* test.
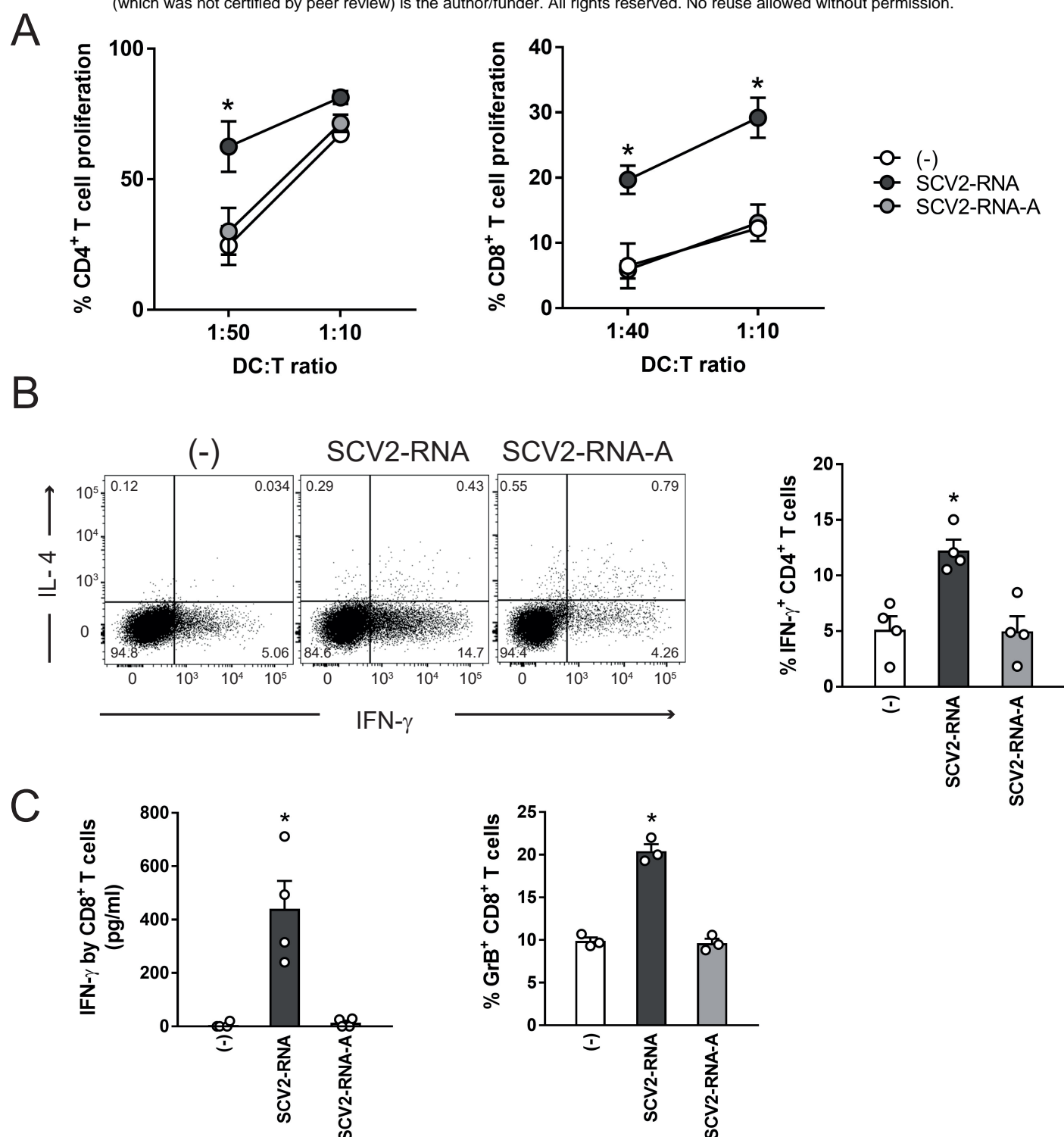
Figure 2. SAMP-activated DCs trigger T cell proliferation and functional activation.
(A) moDCs were stimulated with vehicle (-) or with SCV2-RNA or the A-to-U-replaced SCV2-RNA-A (both at 5 μg/ml) for 24 hours. Activated moDCs were co-cultured for 6 days with CFSE-stained allogenic naïve CD4+ T cells or CD8+ T cells at the indicated DC:T cell ratio. Alloreactive T cell proliferation was assessed by measuring CellTrace-CFSE dye loss by flow cytometry. Data are expressed as mean ± SEM (n=3) of the percentage of proliferating T cells. (B) moDCs stimulated as in (A) were cocultured for 6 days with allogenic naïve CD4+ T (DC:T cell ratio 1:20). Intracellular IFN-γ and IL-4 were evaluated by FACS analysis. Left, dot plots from one representative experiment. Right, bar graphs from four independent experiments. Data are expressed as mean ± SEM of the percentage of IFN-γ-producing cells. (C) moDCs activated as in (A) were cocultured for 6 days with allogenic CD8+ T (DC:T cell ratio 1:10). IFN-γ production was evaluated by ELISA in cell-free supernatants and intracellular Granzyme B (GrB) by FACS analysis. Data are expressed as mean ± SEM (n=3). (A-C) *P< 0.05 versus (-) by one-way ANOVA with Dunnett's post-hoc test.
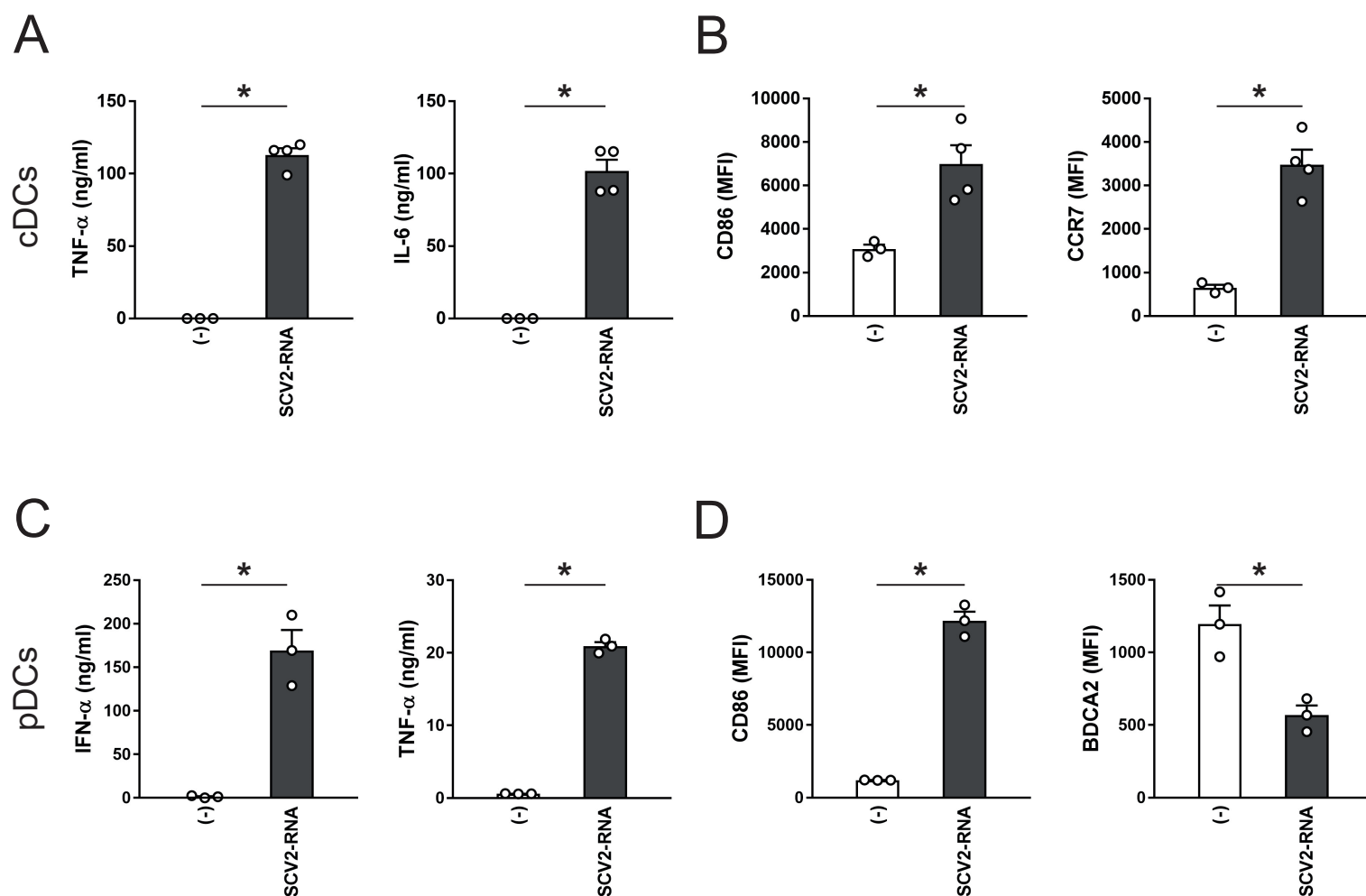
Figure 3. SAMPs activate cytokine secretion and phenotypical maturation in primary circulating DC subsets.

cDCs (2×10^6/ml) and pDCs (1×10^6/ml) were stimulated with 5 µg/ml SCV2-RNA for 24 hours. (A-C) Cytokine secretion was evaluated by ELISA. Data are expressed as mean $\pm$ SEM (n=3-4); *P< 0.05 versus (-) by paired Student's *t* test. (B-D) Surface expression of CD86, CCR7 and BDCA2 was evaluated by FACS analysis. Data are expressed as mean $\pm$ SEM (n=3-4) of the median fluorescence intensity (MFI); *P< 0.05 versus (-) by paired Student's *t* test.
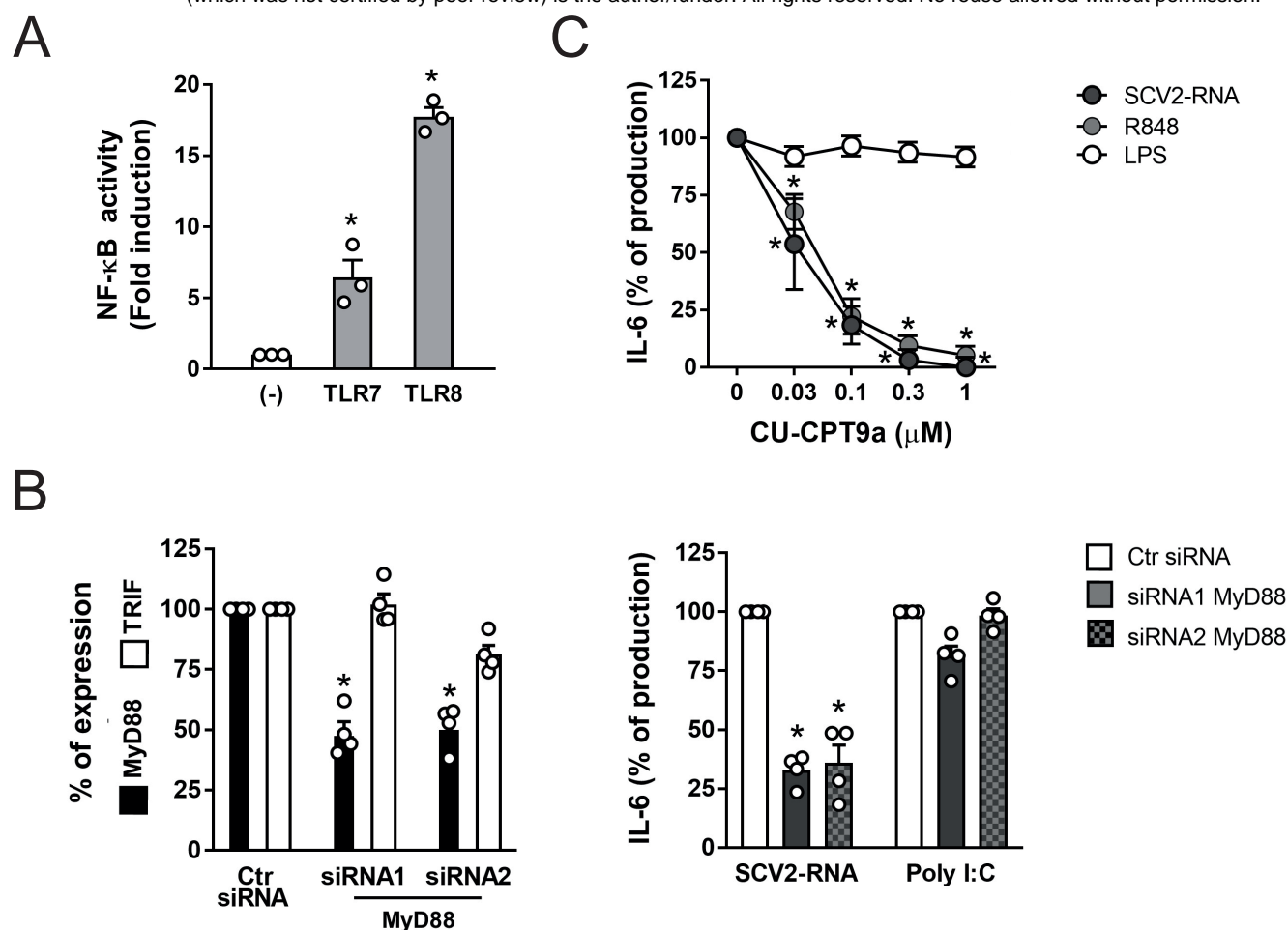
Figure 4. TLR7 and TLR8 are responsible for moDC activation by SAMPs. (A) Reporter HEK-293 cells stably transfected with human TLR7, TLR8 or luciferase alone (-) were stimulated with 10 µg/ml SCV2-RNA for 24 hours. NF-κB activation was evaluated in terms of luciferase activity. Data are expressed ad mean $\pm$ SEM (n=3); *P< 0.05 versus (-) by one-way ANOVA with Dunnett's post-hoc test. (B, left panel) moDCs were transfected with MyD88-specific siRNAs or with control siRNA and the expression of MyD88 and TRIF was evaluated by Real-time PCR. Results are expressed as percentage of expression of MyD88 (black bars) and TRIF (white bars) in cell transfected with control siRNA (mean $\pm$ SEM n=4); *P< 0.05 versus respective "ctr siRNA" by one-way ANOVA with Dunnett's post-hoc test. (B, right panel) moDCs transfected with MyD88-specific siRNAs or with control siRNA were stimulated with 5 µg/ml SCV2-RNA or 25 µg/ml Poly I:C for 24 hours. The production of IL-6 was evaluated by ELISA. Data are expressed as percentage of production for each individual stimulation (n=4); *P< 0.05 versus respective "ctr siRNA" by one-way ANOVA with Dunnett's post-hoc test. (C) moDCs were pre-treated with increasing concentration of CU-CPT9a for 1 hour and then stimulated with SCV2-RNA (5 µg/ml) or R848 (1 µg/ml) or LPS (100 ng/ml) for 24 hours. IL-6 production was evaluated by ELISA. Data are expressed as percentage of production for each individual stimulation (n=3); *P< 0.05 versus respective "0" by one-way ANOVA with Dunnett's post-hoc test.
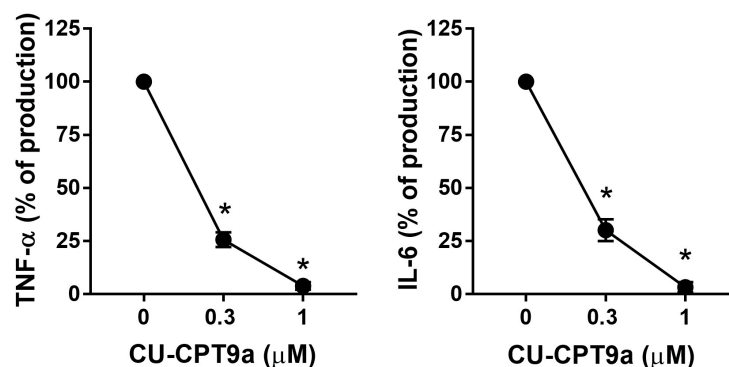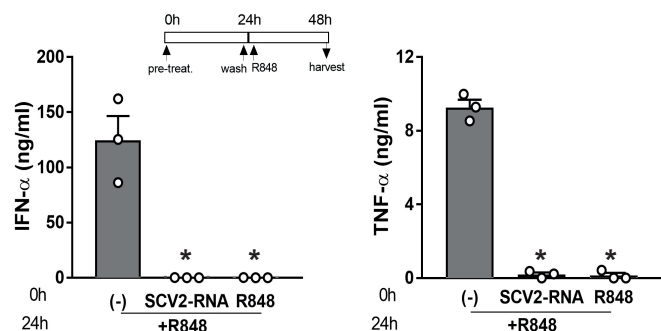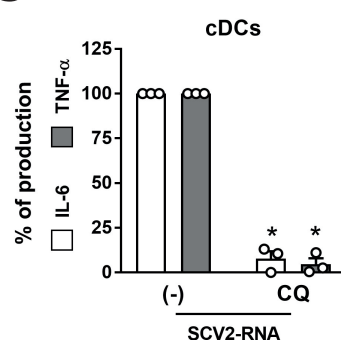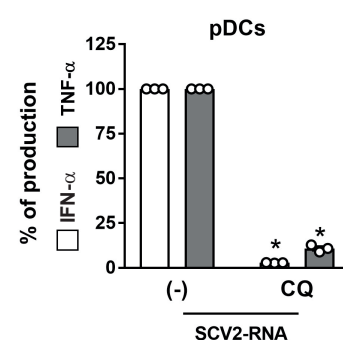
Figure 5. TLR7 and TLR8 are responsible for primary DC activation by SAMPs. (A) cDCs were pre-treated with increasing concentration of CU-CPT9a for 1 hour and then stimulated with SCV2-RNA (5 μg/ml) for 24 hours. Secreted TNF-α and IL-6 were quantified by ELISA. Data are expressed as percentage of production (n=3); *$P < 0.05$ versus "0" by one-way ANOVA with Dunnett's post-hoc test. (B) pDCs were pre-treated (0h) with SCV2-RNA (5 μg/ml) or R848 (1 μg/ml) or left untreated for 24 hours, washed and restimulated with R848 for additional 24 hours. Secreted IFN-α and TNF-α were quantified by ELISA. Data are expressed as mean ± SEM (n=3); *$P < 0.05$ versus "(-)" by one-way ANOVA with Dunnett's post-hoc test. (C) cDCs were pre-treated for 1 hour with Chloroquine (CQ, 10 μM) and then stimulated with SCV2-RNA (5 μg/ml) for 24 hours. Secreted IL-6 (white bars) and TNF-α (grey bars) were evaluated by ELISA. Data are expressed as percentage of production (n=3); *$P < 0.05$ versus respective "(-) SCV2-RNA" by paired Student's *t* test. (D) pDCs were pre-treated for 1 hour with CQ (10 μM) and then stimulated with SCV2-RNA (5 μg/ml) for 24 hours. Secreted IFN-α (white bars) and TNF-α (grey bars) were quantified by ELISA. Data are expressed as percentage of production (n=3); *$P < 0.05$ versus respective "(-) SCV2-RNA" by paired Student's *t* test.
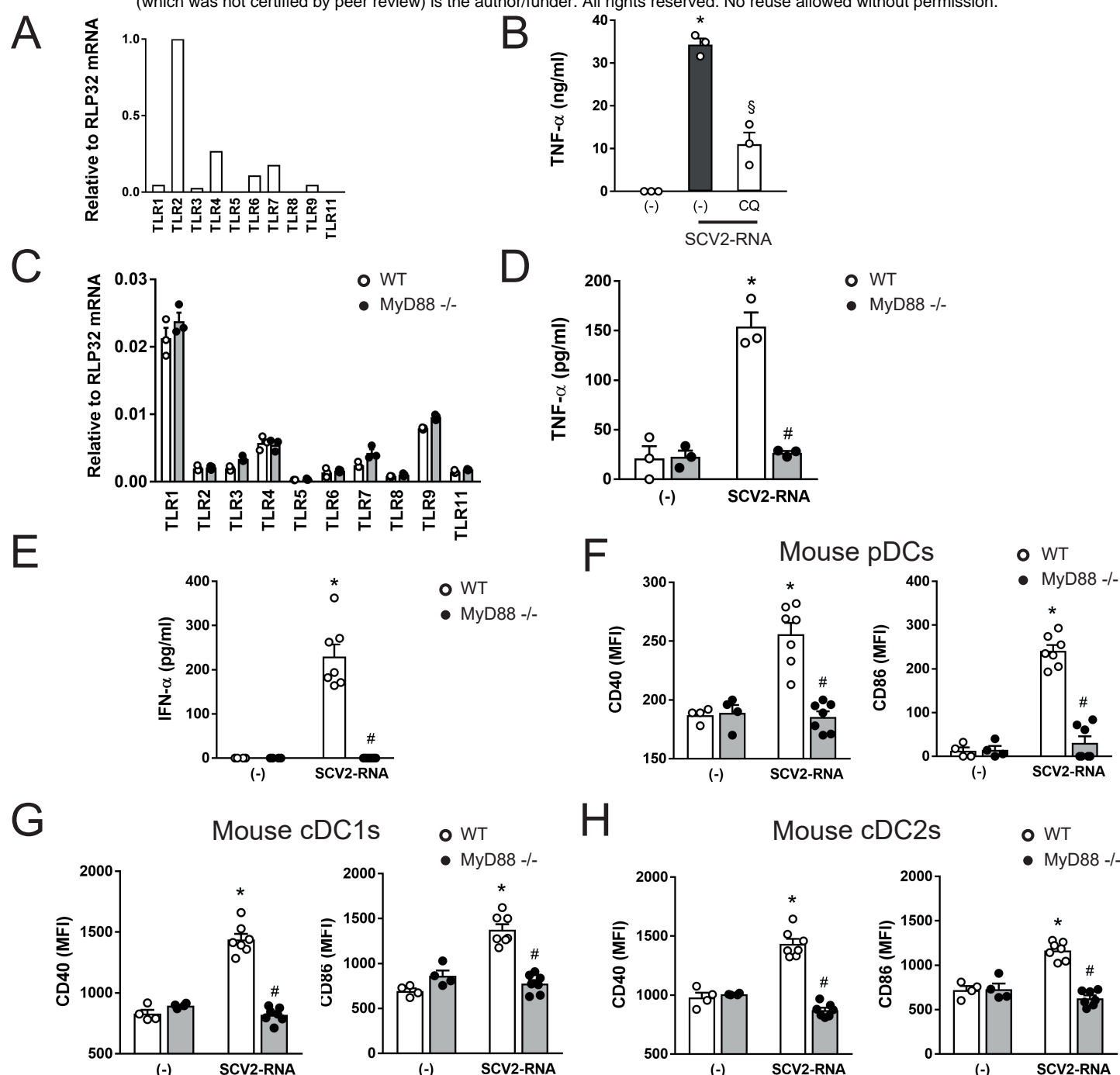
Figure 6. SAMPs activate murine cells *in vitro* and *in vivo*. (A) Expression of TLR mRNAs in RAW264.7 cells. Data are expressed as $2^{-\Delta Ct}$ relative to RPL32 of one representative experiment out of three. (B) RAW264.7 (1×10^6/ml) were pre-treated for 1 hour with CQ (12.5 μM), then stimulated with 5 μg/ml SCV2-RNA or vehicle (-) for 24 hours. Secreted TNF-α was evaluated by ELISA. Data are expressed as mean $\pm$ SEM (n=3); *P< 0.05 versus (-); §P<0.05 versus "(-) SCV2-RNA" by paired Student's *t* test. (C) Expression of TLR mRNAs in splenocytes from WT (white circle) or MyD88$^{-/-}$ mice (black circle). Data are expressed as mean $\pm$ SEM (n=3) of $2^{-\Delta Ct}$ relative to RPL32 of one representative experiment out of three. (D) Splenocytes (3×10^6/ml) from WT (white circle) or MyD88$^{-/-}$ mice (black circle) were stimulated with 5 μg/ml SCV2-RNA or vehicle (-) for 24 hours. Secreted TNF-α was evaluated by ELISA. Data are expressed as mean $\pm$ SEM (n=3); *P< 0.05 versus (-) or #P < 0.05 versus "SCV2-RNA MyD88$^{-/-}$" by paired Student's *t* test. (E) Circulating IFN-α in WT (white circle) or MyD88$^{-/-}$ mice (black circle) treated with SCV2-RNA or vehicle (-) for 6 hours. Data are expressed as mean $\pm$ SEM ((-) n=4, SCV2-RNA n=7); *P< 0.05 versus (-) or #P < 0.05 versus "SCV2-RNA MyD88$^{-/-}$" by unpaired Student's *t* test of one representative experiment out of three. (F-H) Activation of splenic pDCs (CD11c^{int}MHC-II$^+$B220$^+$SiglecH$^+$) (F), cDC1s (CD11c$^+$MHC-II$^+$CD8α$^+$CD11b$^-$) (G) or cDC2s (CD11c$^+$MHC-II$^+$CD8α$^-$CD11b$^+$) (H) from WT (white circle) or MyD88$^{-/-}$ mice (black circle), treated with SCV2-RNA or vehicle (-) for 6 hours evaluated in terms of CD40 and CD86 expression. Data are expressed as mean $\pm$ SEM of the median fluorescence intensity (MFI) ((-) n=4, SCV2-RNA n=7); *P< 0.05 versus (-) or #P < 0.05 versus "SCV2-RNA MyD88$^{-/-}$" by unpaired Student's *t* test.
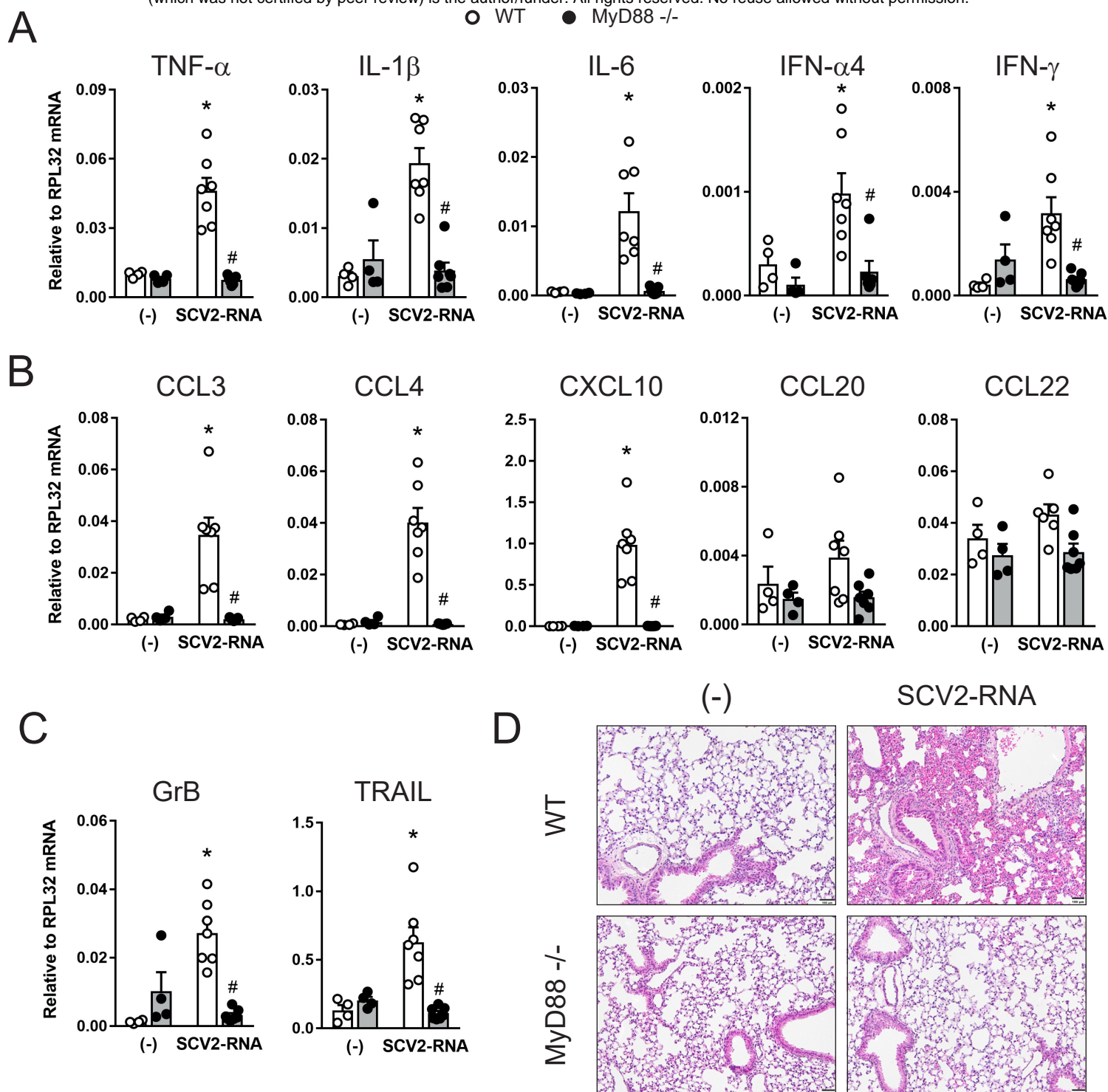
Figure 7. SAMPs induce inflammation *in vivo*. (A-C) Real-time PCR for cytokines, chemokines and effector proteins in lungs of WT (white circle) or MyD88^{-/-} (black circle) treated or not with SCV2-RNA for 6 hours. Data are expressed as mean $\pm$ SEM ((-) n=4, SCV2-RNA n=7) of $2^{-\Delta Ct}$ relative to housekeeping mRNA (RPL32); *P< 0.05 versus (-) or #P < 0.05 versus "SCV2-RNA MyD88^{-/-}" by unpaired Student's *t* test. (D) Histological evaluation of lungs from WT or MyD88^{-/-} mice treated or not with SCV2-RNA for 6 hours. One representative section is shown. Scale bars = 100 μm.